J Mol Model (2012) 18:2369–2376
DOI 10.1007/s00894-011-1259-1

ORIGINAL PAPER

Crystal structure, detonation performance, and thermal stability of a new polynitro cage compound: 2, 4, 6, 8, 10, 12, 13, 14, 15-nonanitro-2, 4, 6, 8, 10, 12, 13, 14, 15-nonaazaheptacyclo [5.5.1.1^{3,11}. 1^{5,9}] pentadecane

Jian-ying Zhang · Hong-chen Du · Fang Wang · Xue-dong Gong · San-jiu Ying

Received: 16 June 2011 / Accepted: 23 September 2011 / Published online: 12 October 2011

Abstract A new polynitro cage compound 2, 4, 6, 8, 10, 12, 13, 14, 15-nonanitro-2, 4, 6, 8, 10, 12, 13, 14, 15-nonaazaheptcyclo [5.5.1.1^{3,11}. 1^{5,9}] pentadecane (NNNAHP) was designed in the present work. Its molecular structure was optimized at the B3LYP/6-31 G(d,p) level of density functional theory (DFT) and crystal structure was predicted using the Compass and Dreiding force fields and refined by DFT GGA-RPBE method. The obtained crystal structure of NNNAHP belongs to the *P-1* space group and the lattice parameters are a=9.99 Å, b=10.78 Å, c=9.99 Å, α=90.01°, β=120.01°, γ=90.00°, and Z=2, respectively. Based on the optimized crystal structure, the band gap, density of state, thermodynamic properties, infrared spectrum, strain energy, detonation characteristics, and thermal stability were predicted. Calculation results show that NNNAHP has detonation properties close to those of CL-20 and is a high energy density compound with moderate stability.

Keywords Cage compound · Crystal structure · Detonation property · DFT · Stability

Introduction

Nowadays, searching for novel high energy density materials (HEDMs) to meet the future energy and military demands has become one of the most active areas. Some candidates of HEDMs with cage structures, e. g., hexanitrohexaazaisowurtzitane (CL-20), polynitroadamantanes, octanitrocubane, and 4-trinitroethyl-2, 6, 8, 10, 12-pentanitrohexaazaisowurtzitane (TNE-CL-20) have been developed and studied [1–8]. They possess characteristics of good explosives, such as high positive heat of formation (HOF), good thermal stability, high crystal density, and enhanced oxygen balance by nitro groups. Therefore, their detonation performance is perfect because of the large quantity of gas products and large energy release on explosion due to high HOF and high strain energies raised by the cage framework.

To find new candidates of HEDM, it is necessary and important to predict the properties and performance of the proposed structures before the laborious and expensive synthesis [9, 10]. Theoretical screening of notional materials allows for elimination of poor candidates and identification of promising HEDM candidates for further consideration, and thus reducing the costs associated with synthesis and evaluation of the materials [11–13]. In the past years, our group has carried out a series of studies on the quantitative estimation of the properties of explosives, such as heat of formation, thermodynamic properties, crystal density, detonation velocity, detonation pressure, and sensitivity [2–4, 8, 14–22] and provided some theoretical basis for selecting promising HEDM candidates for experimental synthesis.

Since, as we know, most high-energy materials are in condensed phases, especially in crystal form, and many physical and chemical properties are tightly related with the crystal packing and morphology, therefore, prediction of crystal structure from the molecular geometry is of greater value.

Enlightened by CL-20 and its substituted derivative TNE-CL-20, a new structure with a different symmetrical

J.-y. Zhang · H.-c. Du · F. Wang · X.-d. Gong (✉) · S.-j. Ying (✉)
School of Chemical Engineering,
Nanjing University of Science and Technology,
Nanjing 210094, People's Republic of China
e-mail: gongxd325@mail.njust.edu.cn
e-mail: yingzijian_luo@163.com

cage, 2, 4, 6, 8, 10, 12, 13, 14, 15-nonanitro-2, 4, 6, 8, 10, 12, 13, 14, 15-nonaazaheptcyclo [5.5.1.1^{3,11}.1^{5,9}] pentadecane (NNNAHP) has been designed (Fig. 1). Its structural and energetic properties, such as crystal packing, thermodynamic properties, strain energy, detonation performance, and thermal stability have been studied using density functional theory (DFT) in combination with molecular mechanics (MM) method. Different from previous investigations focused on the modification of structure with substitutents [8, 18, 20, 22], this work studies the compound with a different cage from that of CL-20 and finds the possibility as HEDMs of this kind of cage compounds.

Computational methods and details

Molecular structure was first optimized at the B3LYP/6-31 G (d,p) level of DFT using Gaussian 03 program package[23]. Two widely-used flexible force fields suitable for organic molecular crystals, Compass [24] and Dreiding [25], were adopted to predict the crystal structure. Polymorph module in Materials Studio package [26] was employed.

According to the statistical data of crystals in the Cambridge Crystallographic Data Centre (CCDC) [27–30], more than 80% of organic crystals belong to seven typical space groups ($P2_1/c$, P-1, $P2_12_12_1$, $Pbca$, $C2/c$, $P2_1$, and $Pna2_1$). It is beneficial to finding the possible crystal structure through a global search consisting of the following steps:

(i) Crystal structures are built and randomly modified using simulation annealing method;
(ii) The structures resulted from (i) are clustered to eliminate duplicates;
(iii) The structures are energy minimized;
(iv) The optimized structures are clustered again to remove duplicates that converged to the same minimum during energy minimization.

The search is repeated separately for each space group. The polymorph with the lowest energy, i.e., the most probable crystal structure of the compound can be found.

DFT GGA-RPBE method [31], a band-by-band conjugate gradient technique, has been used to minimize the total energy of the crystal with respect to the plane-wave coefficients. The cutoff energy of plane waves was set to

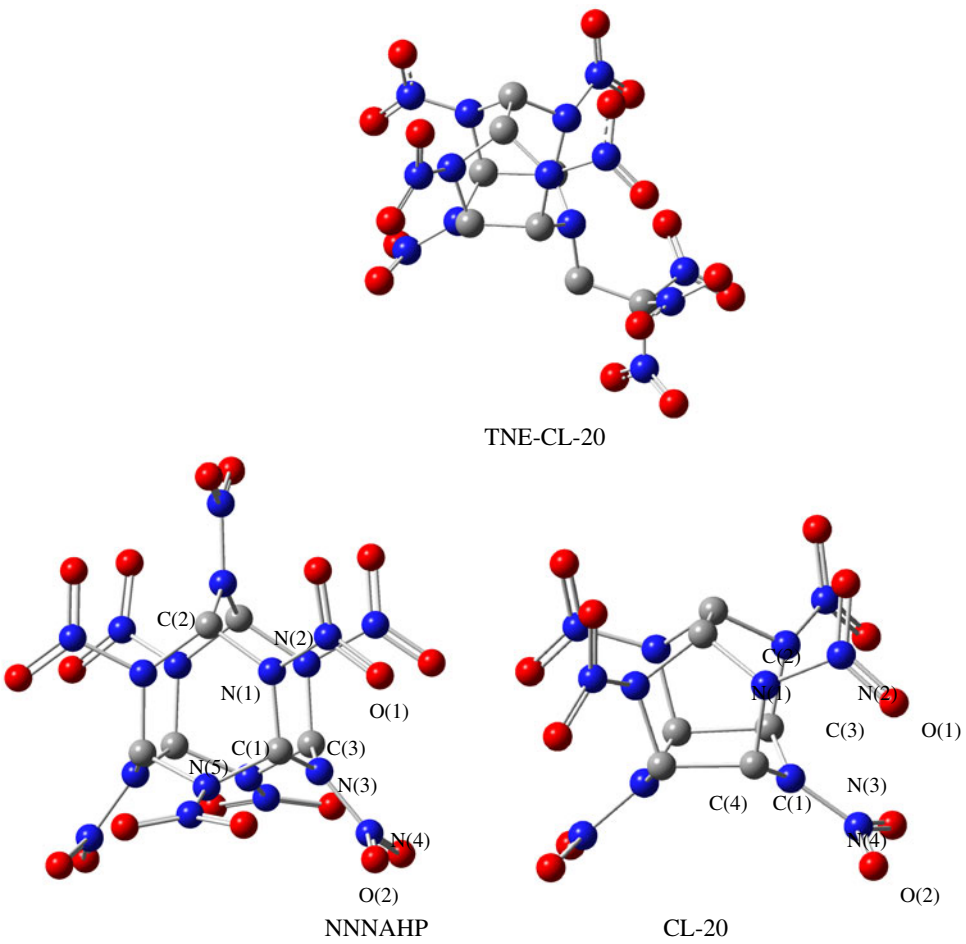

Fig. 1 Illustration of molecular structures of NNNAHP and CL-20 (hydrogen atoms omitted)

Table 1 Possible molecular packing for NNNAHP in seven most possible space groups from the Compass force field

Space groups	$P2_1/c$	$P2_12_12_1$	P-1	$Pbca$	$C2/c$	$Pna2_1$	$P2_1$
Z	4	4	2	8	8	6	3
E(kJ·mol^{-1}·cell^{-1})	−5155.99	−5152.68	−5155.99	−5150.68	−5148.21	−5152.60	−5155.99
ρ(g·cm^{-3})	2.205	2.225	2.206	2.222	2.252	2.219	2.205
a(Å)	17.29	18.28	14.69	16.08	15.90	18.29	9.99
b(Å)	10.78	9.36	9.99	16.08	8.72	9.41	10.78
c(Å)	19.97	7.84	9.99	13.77	32.73	10.76	9.99
α(°)	90.00	90.00	120.05	90.00	90.00	90.00	90.00
β(°)	150.00	90.00	70.10	90.00	126.53	90.00	120.00
γ(°)	90.00	90.00	132.82	90.00	90.00	90.00	90.00

300.0 eV. Brillouin zone sampling was performed using the Monkhost-Pack scheme with a k-point grid of 2×2×2. The total energy of the system was converged to less than 2.0×10^{-5} eV, the residual force less than 0.05 eV/Å^{-1}, the displacement of atoms less than 0.002 Å, and the residual bulk stress less than 0.1 GPa. The band gap, density of state (DOS), and thermodynamic properties were predicted based on the optimized crystal structure using CASTEP code [32].

Ring strain and strain energy (*SE*), important concepts in structural organic chemistry [33–35], can provide a basis that helps to correlate structures, stabilities and reactivities of molecules. The general method for calculating SE of a compound is constructing a reaction in which the compound is the reactant and the product has a 'broken-down' form without strain. Various reactions ranging from isogyric [36] to isodesmic [36] to homodesmotic forms [37] (in order of increasing accuracy) have been used in literature. The general accuracy level aspired to in the literature are homodesmotic reaction schemes [38–42] in which not only the number of various bonds are conserved but also the valence environment around each atom is preserved to raise the advantage of canceling of systematic errors [43]. In the present work, the homodesmotic reaction designed for calculating the SE and HOF of the title compound at the B3LYP/6-31 G(d,p) level is as follows:

$$C_6H_6O_{18}N_{18} + 24CH_3NH_2 \rightarrow 9CH_3N(NO_2)CH_3 + 12NH_2CH_2NH_2 \quad (1)$$

For comparison, the SE and HOF of CL-20 have also been calculated using the following designed homodesmotic reaction:

$$C_6H_6O_{12}N_{12} + 24CH_3NH_2 \rightarrow 3CH_3CH_3 + 6CH_3N(NO_2)CH_3 + 12NH_2CH_2NH_2 \quad (2)$$

The changes in energy, with the correction of zero-point vibrational energy (*ZPE*) of reactions (1) and (2) are the SEs of the title compound and CL-20, respectively:

$$\Delta E = \sum E_0(\text{product}) - \sum E_0(\text{reactant}) + \Delta ZPE \quad (3)$$

The empirical Kamlet-Jacobs equations [13] widely employed [2–4, 14–22] to estimate the detonation velocity and detonation pressure, the important parameters reflecting the explosive performance of energetic materials were used:

$$D = 1.01(N\overline{M}^{1/2}Q^{1/2})^{1/2}(1 + 1.30\rho) \quad (4)$$

Table 2 Possible molecular packing for NNNAHP in seven most possible space groups from the Dreiding force field

Space groups	$P2_1/c$	$P2_12_12_1$	P-1	$Pbca$	$C2/c$	$Pna2_1$	$P2_1$
Z	4	4	2	8	8	6	3
E(kJ·mol^{-1}·cell^{-1})	336.89	372.70	336.01	373.03	369.23	373.08	371.78
ρ(g·cm^{-3})	2.023	1.985	2.039	1.972	2.022	1.988	1.988
a(Å)	6.55	17.12	6.57	18.63	9.83	18.29	6.54
b(Å)	19.10	6.52	16.28	17.45	16.92	9.41	10.12
c(Å)	17.33	18.54	10.09	12.81	26.54	10.76	16.47
α(°)	90.00	90.00	83.47	90.00	90.00	90.00	90.00
β(°)	111.12	90.00	72.27	90.00	66.91	90.00	71.37
γ(°)	90.00	90.00	79.26	90.00	90.00	90.00	90.00

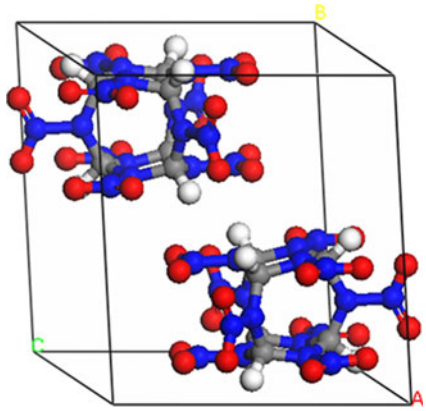

Fig. 2 Crystal structure of NNNAHP in *P*-1 space group

$$P = 1.558\rho^2 N\overline{M}^{1/2}Q^{1/2} \quad (5)$$

where D is detonation velocity ($km \cdot s^{-1}$), P is detonation pressure (GPa), ρ is the density of explosive ($g \cdot cm^{-3}$), N is the moles of gaseous detonation products per gram of explosives, $\overline{M}$ is the average molecular weight of the detonation products, and Q is the detonation energy ($cal \cdot g^{-1}$). N,$\overline{M}$, and Q are determined based on the most exothermic principle.

Bond dissociation energy (*BDE*), the difference between the energies of the parent molecule and the corresponding radical products for a unimolecular bond dissociation reaction which can be used to evaluate the pyrolysis mechanism and thermal stability [3, 8, 14, 15, 20, 21, 44, 45] has been calculated for all possible initial bonds using the following equation:

$$BDE(\mathrm{AB}) = [HOF(\mathrm{A}\bullet) + HOF(\mathrm{B}\bullet)] - HOF(\mathrm{AB}), \quad (6)$$

where AB is the parent molecule, and A· and B· are the corresponding radical products produced by breaking the A—B bond.

Results and discussion

Crystal structure prediction

As shown in Table 1, the energies of various polymorphs obtained with Compass force field range from −5155.99 to −5148.21 $kJ \cdot mol^{-1} \cdot cell^{-1}$. The energies of the structures with the $P2_1/c$, P-1, and $P2_1$ space groups are essentially the same, with the density of P-1 structure being slightly larger. Therefore, under the force field of Compass, the packing of NNNAHP has possibly the P-1 space group.

From Table 2 one sees that the energies of polymorphs in seven space groups obtained with Dreiding force field are in the range of 336.01–373.08 $kJ \cdot mol^{-1} \cdot cell^{-1}$. Once again, the crystal structure with the P-1 space group has the lowest energy. Therefore, the most possible space group of NNNAHP predicted by both force fields is the same.

Figure 2 shows the crystal structure of NNNAHP with the P-1 space group optimized using DFT GGA-RPBE method. The obtained lattice parameters are a=9.99 Å, b=10.78 Å,

Table 3 Selected bond lengths (Å) and angles (°) of NNNAHP and CL-20

	NNNAHP	CL-20		NNNAHP	CL-20
C(1)–N(1)	1.450	1.470	C(1)–N(1)–C(2)	126.23	109.84
C(1)–N(3)	1.448	1.44	C(1)–N(3)–C(3)	129.93	117.67
N(1)–N(2)	1.468	1.442	N(1)–C(1)–N(3)	113.40	114.07
N(3)–N(4)	1.420	1.418	N(1)–C(1)–N(5)	110.84	100.40*

* N(1)–C(1)–C(4)

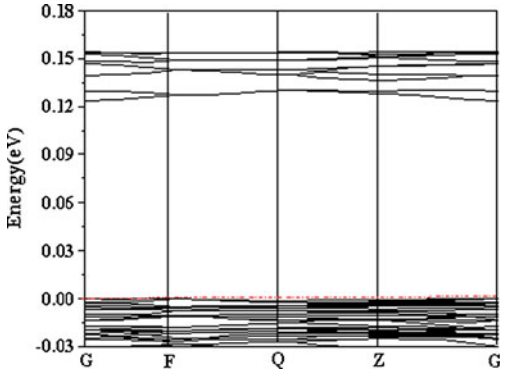

Fig. 3 The bands of NNNAHP along the different symmetric direction of the Brillouin zone

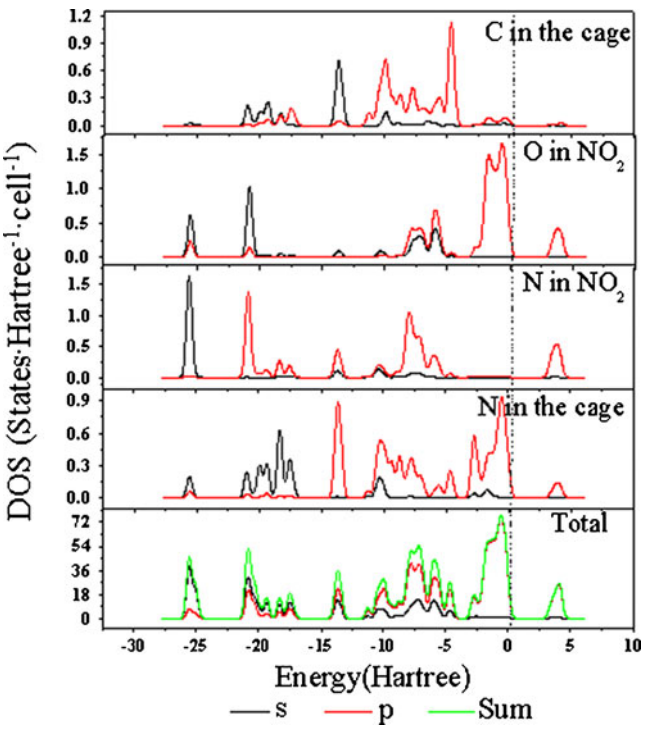

Fig.4 DOS and PDOS of NNNAHP

Table 4 Bond populations for NNNAHP in crystal state

Bond	C(1)-N (1)	C(1)-N (3)	N(2)-O (1)	N(4)-O (2)	N(1)-N (2)	N(3)-N (4)
Population	0.70	0.70	0.80	0.82	0.64	0.66

c=9.99 Å, α=90.01°, β=120.01°, γ=90.00°, Z=2, and ρ= 2.206 g·cm^{-3}, respectively. Some bond lengths and angles are listed in Table 3 including those of CL-20 for comparison. Obviously, there is no big difference in corresponding bond lengths between NNNAHP and CL-20. The noteworthy difference is that N(1)–N(2) is longer in NNNAHP than in CL-20. Since N(1)–N(2) is the trigger bond of CL-20 [46], this may imply that the trigger bond of NNNAHP is weaker and NNNAHP is less stable than CL-20. Further analysis of the bond angles shows that bond angles in the cage of NNNAHP deviate more significantly than those of CL-20 from the normal magnitudes of sp^3 hybrid C or N. This seems to show that both NNNAHP and CL-20 experience strain to some extent but the SE of NNNAHP is larger.

Band gap

The energy gap between the highest occupied molecular/crystal orbital (HOMO/ HOCO) and lowest unoccupied molecular/ crystal orbital (LUMO/LUCO) is tightly related with the impact sensitivity [47–52] and can be used as a criterion to predict the sensitivity of energetic materials with similar structure. It has been well illustrated [48, 49] that the smaller the band gap is, the larger the sensitivity will be. In fact, "the principle of easiest transition (PET)" has already been suggested to predict the relative sensitivity based on the band structures of, e.g., metal-azides crystals [47]. PET is useful not only for the ionic crystals [48–51], but also for the molecular crystals [47, 52]. Figure 3 presents the band structure of the predicted crystal structure using the GGA-RPBE method.

As indicated in Fig. 3, a large gap usually found for nonmetallic compounds exists between the conduction (unoccupied crystal orbitals) and valence (occupied crystal orbitals) bands of NNNAHP. The value of the gap

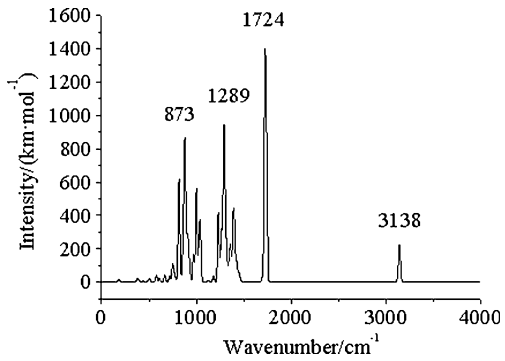

Fig. 5 The calculated infrared spectrum for NNNAHP

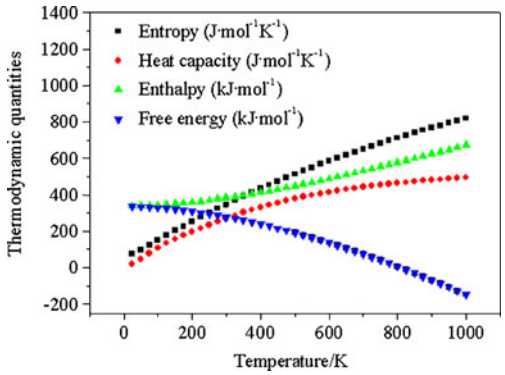

Fig. 6 Thermodynamic properties of the crystal NNNAHP

(3.266 eV) is slightly smaller than that of ε-CL-20 (3.522 eV) [53] but larger than that of HMX (3.160 eV) [54].

Density of state (DOS)

Density of state (DOS) is an important indicator of band structure and the performance of materials. The PDOS obtained by projecting DOS on atom-centered orbital can help us understand the band structure and the constitution of energy bands better. Figure 4 gives the DOS and PDOS of the predicted crystal structure of NNNAHP using the GGA-PBE method.

From Fig. 4, we note that the valence bands of NNNAHP are mainly contributed from the p orbitals of O atom in NO_2 and N atom in the cage frame (i.e., nitramine nitrogen) while the conduction bands are mainly composed of the p orbitals of N and O atoms of NO_2 groups, together with a little contribution of the p orbitals of N atom in the cage. These show that the N–NO_2 bond in the title compound acts as an active center and may be the initial breaking bond in the pyrolysis steps, as was found for CL-20 [46].

Bond populations

Table 4 shows some bond populations for the crystalline NNNAHP. Bond population is a measure of the strength of a bond between two atoms. A high value of the bond population indicates a strong bond, and vice versa. The bond populations of C–N, N=O, and N–NO_2 are 0.70, 0.80~0.82, and 0.64~0.66, respectively, implying the strength of the bonds is N=O>C–N>N–NO_2, i.e., N–NO_2 is the weakest bond in the molecule of NNNAHP, which agrees with the previous speculation from DOS that N–NO_2 may be the trigger bond in the pyrolysis.

Infrared spectrum

Figure 5 provides the simulated IR spectrum of NNNAHP based on the scaled harmonic vibrational frequencies. Due

Table 5 HOFs and SEs for NNNAHP and CL-20 obtained from reactions (1) and (2)

Compound	E_0[a] /(a.u.)	*ZPE*/(a.u.)	*HOF*/(kJ·mol^{-1})	*SE*/(kJ·mol^{-1})
$CH_3N(NO_2)\ CH_3$	−339.66462	0.095425	−82.98[b]	/
$NH_2CH_2NH_2$	−151.21678	0.082327	−78.84[b]	/
CH_3NH_2	−95.86369	0.064218	−80.37[b]	/
CH_3CH_3	−79.83874	0.074942	−84.00[c]	/
NNNAHP	−2570.62076	0.276230	772.45	128.24
CL-20	−1791.18314	0.221315	681.48	107.24

[a]E_0 is the total energy, [b]Obtained at the G3 level from the formation reactions: 2 C(s)+3H_2+O_2+N_2→$CH_3N(NO_2)CH_3$, C(s)+3H_2+N_2→$NH_2CH_2NH_2CH_3$, C(s)+2.5H_2+0.5 N_2→CH_3NH_2, [c]Ref [56]

to the complexity of vibrational modes, only some characteristic bands will be analyzed and discussed. Obviously, there are four main regions in the spectrum. The strongest signal at 1724 cm^{-1} corresponds to the N=O asymmetric stretch of nitro groups. The corresponding calculated and experimental frequencies of CL-20 are 1690 cm^{-1} and 1605 cm^{-1} [55]. The next strong characteristic peak at 1289 cm^{-1} in the range of 1200~1500 cm^{-1} is a complex of N=O symmetric stretch of nitro groups, the skeletal vibration of heterocycle, the stretching vibration of the C–N single bond, and the C–H stretch. For CL-20, this peak is predicted to be near 1250 cm^{-1} [55]. Peaks at less than 1050 cm^{-1} such as 873 cm^{-1} are mainly caused by the deformation of the heterocyclic skeleton, the N–NO_2 stretch, and the bend vibration of the C–H bonds, which are located at the fingerprint region and can be used to identify isomers. The modes in 3100~3150 cm^{-1} are associated with the C–H stretch. In this region the strongest characteristic peak is at 3138 cm^{-1}.

Thermodynamic properties

The thermodynamic functions including enthalpy, entropy, free energy, and heat capacity for the crystal NNNAHP are presented in Fig. 6. With the increase of temperature, the calculated enthalpy monotonically increases because the main contributions to the enthalpy are from the vibrational motion, which, at higher temperature, is intensified and makes more contributions. The same is also true for the entropy and heat capacity. For the free energy, as the temperature increases, the value gradually decreases.

Since the evaluation of explosive performance of energetic materials requires the knowledge of HOF which is also of great importance for researchers involved in thermochemistry, we have calculated the standard HOF of NNNAHP using the homodesmotic reaction (1) as well as the HOF of CL-20 using the homodesmotic reaction (2) for comparison. Table 5 collects the total energies (E_0) and HOFs of the species involved in the reactions. With the data in Table 5, it is easy to obtain the HOFs of NNNAHP and CL-20. The HOF of NNNAHP (772.45 kJ·mol^{-1}) is larger than those of CL-20 (681.48 kJ·mol^{-1}) and TNE-CL-20 (705.61 kJ·mol^{-1}) [8] obtained at the same computational level, which can be attributed to the presence of more NO_2 groups and a higher-strain cage skeleton.

Table 6 Detonation performance of NNNAHP and CL-20

Compound	ρ/(g·cm^{-3})	*D*/(km·s^{-1})	*P*/(GPa)	*Q*/(kJ·g^{-1})
NNNAHP	2.009	9.554	43.136	−6.239
CL-20	1.970[a](2.040[b])	9.730[a](9.381[b])	44.642[a]	−7.269[a] (−6.234[c])

[a] Calculated value from Ref. [62], [b] Experimental value from Ref. [63], [c] Experimental value from Ref. [1]

Strain energy

Many studies [38–42] have proved that computational results of SE at the B3LYP/6-31 G (d,p) via homodesmotic process are reasonable. For example, the SE of norbornane obtained by the homodesmotic method (63.15 kJ·mol^{-1}) [57] is in agreement with experimental value (60.22 kJ·mol^{-1}) [58]. In the present work, the SE of NNNAHP and CL-20 were calculated using the designed homodesmotic reactions (1) and (2).

The results were also collected in Table 5. One sees that SE of NNNAHP (128.24 kJ·mol^{-1}) is larger than that of CL-20 (107.24 kJ·mol^{-1}), which is in agreement with their molecular structure character but much smaller than that of octanitrocubane (1102.50 kJ·mol^{-1}) [59], which indicate that NNNAHP is more strained than CL-20 while less strained than cubane. The SE accounts for about 17% of HOF for NNNAHP, which will be released during detonation and make contributions to detonation energy.

Detonation characteristics

Since density has a significant effect on the predicted detonation performance, we have also calculated the density of NNNAHP using another two methods: In the first method, the density is predicted from the volume inside an electronic isodensity contour of 0.001 e·Bohr^{-3} at the B3LYP/6-31 G(d,p) level. It has been widely adopted and the results are confirmed to be quite reliable. In this study, it gives a density of 2.140 g·cm^{-3}, which is

smaller than that predicted from Compass force field (2.206 g·cm^{-3}). The second one is the method proposed by Politer et al. [60] to improve the results of the above method. The following equation is adopted in this method to predict the density:

$$\rho = \alpha_1\left(\frac{M}{V}\right) + \beta_1\left(\nu\sigma_{tot}^2\right) + \gamma_1 \quad (7)$$

where α_1, β_1, and γ_1 are constants and their value are 0.9183, 0.0028, and 0.0443, respectively. $\frac{M}{V}$ is the density obtained from the first method. ν is a parameter to quantify the degree of balance between the positive and negative potentials on a molecular surface, σ_{tot}^2 is the sum of the positive and negative components, $\sigma_{tot}^2 = \sigma_+^2 + \sigma_-^2$. The result obtained using this method is 2.009 g·cm^{-3}, which is the smallest among the three predicted densities of NNNAHP.

Together with the predicted HOF and the smallest crystal density (2.009 g·cm^{-3}), the detonation velocity, detonation pressure, and detonation energy were calculated by the Kamlet-Jacobs empirical equations [43]. Apparently, the calculated density of NNNAHP (2.009 g·cm^{-3}) is larger than that of CL-20 (1.970 g·cm^{-3}) while the detonation performance of the former are slightly lower than the latter at the same computational level, but still meet the requirements as HEDC (i.e., ρ≈1.9 g·cm^{-3}, D≈9.0 km·s^{-1}, P≈40.0 GPa) [61]. (Table 6)

Pyrolysis mechanism and thermal stability

Thermal stability is a fundamental property of energetic materials. Nitro groups are often the primary cause of initiation reactivity of polynitro compounds [15, 16, 19–21]. Due to the symmetry of the structure of NNNAHP, *BDE*s of two different N–NO_2 bonds with smaller bond populations, i.e., N(1)–NO_2 and N(3)–NO_2 are calculated. The results are 151.85 kJ·mol^{-1} and 177.04 kJ·mol^{-1}, respectively, agreeing with the result that the former has a smaller electron population than the latter and may be the trigger bond in the pyrolysis. The *BDE* of the trigger bond of NNNAHP is somewhat smaller than that of CL-20 (161.38 kJ·mol^{-1}) [46] which is consistent with the fact that the trigger bond N(1)–NO_2 in NNNAHP is longer than that in CL-20, but it is still large enough and suffices the stability request of *BDE* >120 kJ·mol^{-1} suggested previously [61].

Conclusions

A novel high energy compound 2, 4, 6, 8, 10, 12, 13, 14, 15-nonanitro-2, 4, 6, 8, 10, 12, 13, 14, 15-nonaazaheptcyclo [5.5.1.1^{3,11}.1^{5,9}] pentadecane (NNNAHP) has been proposed and the crystal structure, band gap, density of state, infrared spectrum, thermodynamic property, detonation performance, and thermal stability have been predicted in the present work. The predicted HOF, crystal density, and detonation performance of NNNAHP are close to those of CL-20. The N–NO_2 bond is predicted to be the trigger bond during pyrolysis based on the results of DOS, bond populations, and bond dissociation energy. The stability of the title compound is slightly lower than that of CL-20. Calculation results show that NNNAHP deserves attention as a candidate of HEDC. This computational study may provide an incentive for future studies about new cage compounds.

Acknowledgments This work is supported by the National Natural Science Foundation of China (Grant No. 11076017).

References

1. Simpson RL, Urtiew PA, Ornellas DL (1997) Moody GL, Scribner JK, Hoffman DM. Propellants Explos Pyrotech 22:249–255
2. Xu XJ, Xiao HM, Gong XD, Zhu WH (2006) J Phys Chem A 110:5929–5933
3. Xu XJ, Xiao HM, Gong XD, Ju XH, Chen ZX (2005) J Phys Chem A 109:11268–11274
4. Xu XJ, Zhu WH, Gong XD, Xiao HM (2008) Sci China B 51:427–439
5. Kortus J, Pederson MR, Richardson SL (2000) Chem Phys Lett 322:224–230
6. Eaton PE, Gilardi RL, Zhang MX (2000) Adv Mater 12:1143–1148
7. Sun CH, Zhao XQ, Li YC, Pang SP (2010) Chinese Chem Lett 21:572–575
8. Zhang JY, Du HC, Wang F, Gong XD, Huang YS (2011) J Phys Chem A 105:6617–6621
9. Muthurajan H, Sivabalan R, Venkatesan N, Talawar MB, Asthana SN (2003) Computational approaches for performance prediction of high energy materials. In: Proceedings of 4th International High Energy Materials Conference. India, pp 470–486
10. Muthurajan H, Sivabalan R, Talawar MB, Asthana SN (2004) Artificial intelligence methodology for thermodynamic analysis of high energetic materials. In: Proceedings of 14th National Symposium on Thermal Analysis. India, pp 225–228
11. Rice BM, Hare J (2002) Thermochim Acta 384:377–391
12. Miller MS, Rice BM, Kotlar AJ, Cramer RJ (2000) Clean Products Processes 2:37–46
13. Kamlet MJ, Jacobs SJ (1968) Chemistry of detonations.I. A simple method for calculating detonation properties of C–H–N–O explosives. J Chem Phys 48:23–35
14. Zhang J, Xiao HM (2002) J Chem Phys 116:10674–10683
15. Qiu L, Xiao HM, Gong XD, Ju XH, Zhu WH (2006) J Phys Chem A 110:3797–3807
16. Qiu L, Xiao HM, Ju XH, Gong XD (2005) Int J Quantum Chem 105:48–56
17. Xiao HM, Zhang J (2002) Sci China Ser B 45:21–29
18. Ju XH, Xiao HM, Ma XF (2006) Int J Quantum Chem 106:1561–1568
19. Qiu L, Gong XD, Ju XH, Xiao HM (2008) Sci China B 51:1231–1245
20. Wang GX, Shi CH, Gong XD, Xiao HM (2009) J Phys Chem A 113:1318–1326

21. Wang GX, Gong XD, Xiao HM (2009) Int J Quantum Chem 109:1522–1530
22. Qiu LM, Gong XD, Wang GX, Zheng J, Xiao HM (2009) J Phys Chem A 113:2607–2614
23. Frisch MJ et (2003) Gaussian 03, Revision A.1. Gaussian Inc, Pittsburgh, PA
24. Sun H (1998) Compass: an *ab initio* force-field optimized for condense-phase applications-overview with details on alkanes and benzene compounds. J Phys Chem B 102:7338–7364
25. Mayo SL, Olafson BD, Goddard WA III (1990) DREIDING: a generic forcefield. J Phys Chem 94:8897
26. Materials studio 4.4. (2009) Accelrys
27. Mighell AD, Himes VL, Rodgers JR (1983) Acta Crystallogr A 39:737–740
28. Wilson AJC (1988) Space groups rare for organic structures. I. Triclinic, monoclinic and orthorhombic crystal classes. Acta Crystallogr A 44:715–724
29. Srinivasan R (1992) Acta Crystallogr A 48:917–918
30. Baur WH, Kassner D (1992) Acta Crystallogr B 48:356–369
31. Perdew JP, Burke K, Ernzerhof M (1996) Phys Rev Lett 77:3865–3868
32. Segall MD, Lindan PJD, Probert MJ, Pickard CJ, Hasnip PJ, Clark SJ, Payne MCJ (2002) Phys Condens Matter 14:2717–2744
33. Greenberg A, Liebman JF (1978) Strained organic molecules. In: Organic chemistry series 38. Academic Press, New York, pp 1–40
34. Kenneth BW (1986) Angew Chem Int Edn Engl 25:312–322
35. Wheeler SE, Houk KN (2009) Schleyer PvR, Allen WD. J Am Chem Soc 131:2547–2560
36. Hehre WJ, Radom L, PvR S, Pople JA (1986) Ab Initio Molecular Orbital Theory. Wiley, New York
37. George P, Trachtman M, Bock CW, Brett AM (1975) Theor Chim Acta 38:121–129
38. Zhao M, Gimarc BM (1993) J Phys Chem 97:4023–4030
39. Bachrach SM (1989) J Phys Chem 93:7780–7784
40. Magers DH, Davis SR (1999) Comput Theor Chem 487:205–210
41. Lewis LL, Turner LL, Salter EA, Magers DH (2002) Comput Theor Chem 592:161–171
42. Dill JD, Greenberg A, Liebman JF (1979) J Am Chem Soc 101:6814–6826
43. Walker JE, Adamson PA, Davis SR (1999) Comput Theor Chem 487:145–150
44. Yao XQ, Hou XJ, Wu GS, Xu YY, Xiang HW, Jiao H, Li YW (2002) J Phys Chem A 106:7184–7189
45. Shao J, Cheng X, Yang X (2005) Comput Theor Chem 755:127–130
46. Li YJ, Song J et al. (2009) Acta Chim Sinica 67:1437–1446
47. Saraf SR, Rogers WJ, Mannan MS (2003) J Hazard Mater 98:15–29
48. Xiao HM, Li YF (1995) Sci China Ser B 38:538–545
49. Xiao HM, Li YF, Qian JJ (1994) Chin J Chem Phys 10:235–240
50. Zhu WH, Xiao JJ, Xiao HM (2006) J Phys Chem B 110:9856–9862
51. Zhu WH, Xiao JJ, Xiao HM (2006) Chem Phys Lett 422:117–121
52. Zhu WH, Xiao JJ, Ji GF, Zhao F, Xiao HM (2007) J Phys Chem B 111:12715–12722
53. Xu XJ, Zhu WH, Xiao HM (2007) J Phys Chem B 111:2090–2097
54. Ji GF, Xiao HM, Dong HS (2002) Acta Chim Sinica 60:194–199
55. Kholod Y, Okovytyy S, Kuramshina G, Qasim M, Gorb L, Furey J, Honea P, Fredrickson H, Leszczynski J (2006) J Mol Struct 794:288–302
56. Lide DR (ed) (2010) CRC Handbook of Chemistry and Physics, 89th edn. CRC, Boca Raton, FL, 2009, Internet Version
57. Howell J, Goddard JD, Tam W (2009) Tetrahedron 65:4562–4568
58. Wiberg KB (1986) Angew Chem Int Edn Engl 25:312
59. Fan XW, Ju XH, Xia QY, Xiao HM (2008) J Hazard Mater 151:255–260
60. Politzer P, Martinez J, Murray JS, Concha MC, Toro-Labbé A (2009) Mol Phys 107:2095–2101
61. Xiao HM, Xu XJ, Qiu L (2008) Theoretical Design of High Energy Density Materials. Science Press, Beijing
62. Ghule VD, Jadhav PM, Patil RS, Radhakrishnan S, Soman T (2010) J Phys Chem A 114:498–503
63. Sikder AK, Sikder N (2004) J Hazard Mater 112:1–15